Toxicological & Environmental Chemistry
Vol. 92, No. 2, February 2010, 279–299

Taylor & Francis
Taylor & Francis Group

Chronic exposure to Mn inhalation may have lasting effects: A physiologically-based toxicokinetic model in rats

Pamela K. Douglas[a]*, Mark S. Cohen[b] and Joseph J. DiStefanoIII[a]

[a]*Biocybernetics Laboratory, University of California, Los Angeles, CA, USA;* [b]*Department of Psychiatry and Biobehavioral Sciences, David Geffen School of Medicine, University of California Los Angeles, Los Angeles, CA, USA*

(*Received 6 June 2008; final version received 23 January 2009*)

In humans, inhaled manganese (Mn) initiates neurodegeneration in the striatum and produces manganism, a disorder phenotypically mimetic of Parkinson's disease (PD), and it is unclear how Mn has this effect. The main route of inhaled Mn passage to striatum – via direct transneuronal transport via the olfactory system or indirectly via lungs to blood, and the relative contributions of each of these pathways – also remain unclear. The primary goal of this investigation was to explore these questions – and others – quantitatively in a rat model. An 11-compartment whole-body physiologically-based toxicokinetic (PBTK) model of Mn distribution, optimally and simultaneously fitted to a single set of multiorgan rat data was used. The fully quantified model provided numerous kinetic parameters, including the relative distribution of whole-body Mn for each compartment in response to a constant simulated input of inhaled Mn, and the relative contributions of olfactory and pulmonary pathways. The liver, which actively concentrates Mn, was found to contain the greatest percentage (~6.7%). Both the striatum and cerebellum had (~0.1%) of total Mn, which is notable given that striatum volume is approximately 100-fold less than cerebellum. The relative percentages of olfactory (~52%) and pulmonary (~48%) contributions to Mn in striatum were approximately constant computed for up to 200 days after aerosolized exposure. Following simulated acute exposure ($>1\,mg\,Mn/m^3$), clearance from striatum was nearly complete after ~100 days. In a separate simulation of low-level chronic exposure ($\sim 0.01\,mg\,Mn/m^3$), striatal Mn was saturated and reached an approximately steady value at 100 days.

Keywords: manganese; toxicity; kinetic; manganism

Introduction

At homeostatic levels, manganese (Mn) is an essential nutrient, found in many metabolic pathways and enzymes such as pyruvate carboxylase and superoxide dismutase (Teeguarden et al. 2007a). However, at higher levels in humans, Mn concentrates in a region of paleostriatum, the globus pallidus (GP), and produces manganism, a disorder that resembles Parkinson's disease (PD) (Bowler et al. 2006). These neurotoxic effects were first noted in 1837 (Couper 1837), only shortly after the first description of PD in 1817 (Couper 1837). Bradykinesia, resting tremor, psychiatric disturbances, impotence, and postural instability are hallmark clinical features of patients with manganism

*Corresponding author. Email: pamelad@seas.ucla.edu

ISSN 0277–2248 print/ISSN 1029–0486 online

DOI: 10.1080/02772240902830599
http://www.informaworld.com

(Aschner and Aschner 2005), and in some cases, the clinical phenotype is nearly indistinguishable from PD.

Ferro-manganese plants (Wang et al. 1989; Zatta et al. 2003), lead-sulfate batteries (Kuhn et al. 1998), Mn mining, crop dusting of Mn-based pesticides such as mancozeb and maneb (Ascherio et al. 2006; Baldereschi et al. 2007; Zatta et al. 2003), and steel welding, all represent significant risks for human exposure to airborne Mn fumes. Only a small percentage of ingested Mn is absorbed via the gastrointestinal tract, however a much larger portion of aerosolized inhaled Mn reaches the bloodstream (Aschner and Aschner 2005). Acute exposure to high levels of Mn fumes (>1 mg Mn/m^3), or chronic exposure to even smaller amounts of Mn in the aerosol form, are known to induce the adverse effects of Mn (Dobson, Erikson, and Aschner 2004). Inhalation of Mn in the form of aerosols, fumes or suspended particulate matter is now the most recognized occupational hazard for human toxicity (Dobson, Erikson, and Aschner 2004).

Routes of exposure: olfactory versus pulmonary

How aerosolized Mn reaches striatum, and why it preferentially is sequestered in this area of the brain is still not understood (Shinotoh et al. 1997). Several studies have not observed an elevation of Mn in areas of the brain contralateral to intranasal administration, which demonstrates direct olfactory to brain transport of Mn in rats, which breath only through their nose (Brenneman et al. 2000; Dorman et al. 2002a; Gianutsos, Morrow, and Morris 1997). It is well established that Mn^{2+} can mimic calcium transport, and be taken up by voltage gated Ca^{2+} channels in neurons, transported along axons, and then across synapses (Pautler, Mongeau, and Jacobs 2003). In this way, Mn might be transported transneuronally directly from the olfactory receptor cells to striatum, without ever crossing the blood brain barrier (BBB) (Brenneman et al. 2000).

In contrast, other studies suggest that the majority of Mn enters striatum indirectly by an unspecified route, whereby Mn enters the lungs, is taken up by blood and then crosses into brain (Anderson et al. 1999; Crossgrove and Yokel 2005; Crossgrove et al. 2003; Dorman et al. 2002a; Yokel and Crossgrove 2004; Yokel, Crossgrove, and Bukaveckas 2003) possibly via the blood brain barrier (BBB) (Crossgrove et al. 2003; Crossgrove and Yokel 2004, 2005), the blood-cerebrospinal fluid barrier (B-CSFB) (Bock et al. 2008) or by simple diffusion across other areas of the brain in direct contact with blood, such as the area postrema. In certain rare cases, Mn toxicity was observed following IV injection of total parenteral nutrition (TPN), which typically contains Mn in the solution (Aschner and Aschner 2005). Increased Mn in striatum following IV injection into blood is analogous to the indirect lung to blood route, whereby Mn is crossing from blood to brain. In these instances, it is clear that Mn is reaching striatum without ever utilizing the olfactory system, thus supporting the indirect route hypothesis.

Time of residence

To date, the residence time of Mn in striatum has not been assessed accurately in humans, and monkey studies showed only a small quantitative decline in Mn concentration after 248 days (Crossgrove and Zheng 2004). Once Mn enters the human brain, it accumulates in highest concentration in substantia nigra, followed by striatum, hippocampus, and then frontal cortex (Crossgrove and Zheng 2004). Under normal physiologic conditions, the Mn concentration in the human brain ranges between 0.3–0.7 μg/g of wet tissue. Kim

(2006) suggested using presence versus absence of striatal Mn on MRI scans as a first step in triage when manganism is suspected, because of its powerful effect on T1 relaxation rates. Understanding the residence time of striatal Mn following either acute or chronic exposure may therefore be vital for diagnostic sensitivity and staging.

Modeling manganese and other metals

With its ubiquitous use in the fuel additive methylcyclopentadienyl manganese tricarbonyl (MMT) (Kaiser 2002), the consequences of Mn exposure requires further quantitative investigation (Andersen, Gearhart, and Clewell 1999). Kinetic modeling has been done for other metals such as cadmium (Dote et al. 2008), zinc (House and Wastney 1997), mercury (O'Flaherty 1998), nickel (Hack et al. 2007), arsenic (Gentry et al. 2004) and lead (for review see Rabinowitz 1998) in rats. Toxicokinetic (TK) models for Mn have described whole-body Mn clearance rates (Dorman et al. 2002a; Dorman et al. 2006; Takeda, Sawashita, and Okada 1995), brain clearance rates (Calonder et al. 1999), lung clearance rates (Thompson et al. 2006), and biliary uptake and elimination (Teeguarden et al. 2007a; Teeguarden et al. 2007b). More comprehensive analyses for Mn have also been reported in rats (Nong et al. 2008; Teeguarden et al. 2007a; Teeguarden et al. 2007b; Teeguarden et al. 2007c). Teeguarden and others (2007a) used a two-compartment hepato-intestinal model to describe biliary uptake and elimination in rats and reported that rate constants for Mn uptake decreased with increased Mn intake. Additional hepatic modeling focused on quantifying extraction from either orally ingested or systemic Mn (Teeguarden et al. 2007b) and several indices of whole-body kinetics of Mn distribution and elimination in rats (Nong et al. 2008; Teeguarden et al. 2007c).

The present study focuses on development and extensive quantification of a new whole-body physiologically-based toxicokinetic (PBTK) compartmental model of Mn in rats. It is based on known rat physiology (Farris and Griffith 1949), neuroanatomy (Zeman 1963) and published multiorgan kinetic data (Dorman et al. 2002a), and provides new information about Mn entry routes to subcortical structures, Mn whole-body steady state distribution, and striatal Mn levels following either acute or chronic exposure.

Methods

Kinetic data for model construction and quantification

The new PBTK model was quantified using published radioactive Mn concentration (nCi per gram ± S.E.M.) data at six time points in 250 g 8-week-old pups, measured in olfactory epithelium, olfactory tract, olfactory bulb, residual brain (brain-resto), cerebellum, striatum, pancreas, liver, kidneys, testes, and lungs, using gamma spectrography following 90 min exposure to $^{54}MnHPO_4$ (Dorman et al. 2002a). Radioactive concentration data (nCi/g wet weight) was converted to Mn mass using the following equation:

$$\mathrm{Mass_{Mn}\ (mg)} = \left(\frac{\mathrm{TR\left(nCi^{54}Mn/(g \times tww)\right) tww_{organ}\ (g)}}{\mathrm{SA(nCi/mg)}} \right), \tag{1}$$

where, TR is tissue radioactivity, specific activity (SA) was 0.51×10^{-6} nCi/mg Mn, and tww is the tissue wet weight of the specific organ, calculated specifically for CD rat

with mean mass of 250 g, as was used in the Dorman et al. (2002a) study. The weights of olfactory epithelium and tract were obtained from Zivic Laboratories, who measured these organs in rats matched for age and weight. Mn masses for each brain region or organ were obtained as follows. For the olfactory bulb and cerebellum, conversions to mass units were based on these brain regions occupying approximately 4 and 10% of the rat brain, respectively (Swanson 1995). Percent organ weights from Clodfelder, Chang, and Vincent (2004) were used for all other rat organs. Animals were fed a nonradioactive diet. Since only a ~1–3% of orally ingested Mn is absorbed by the gastrointestinal tract (Aschner and Aschner 2005), it was assumed that any recirculated $^{54}MnHPO_4$ from gut was negligible. The Mn entry route to the brain from blood is unknown, so our initial model hypothesis permitted multiple routes of entry from lung-to-blood-to-brain, namely via the blood brain barrier (BBB), the blood cerebrospinal fluid barrier (BCSFB) via the choroid plexuses, as well as direct input via the nasal cavity and olfactory tract. Biliary clearance accounts for >95% of Mn elimination (Crossgrove and Zheng 2004).

Model simulation and parameter estimation methods

Preliminary explorations with the data

The program W^{3}DIMSUM (Harless and Distefano 2005) was used to fit some organ data sets to multiexponential models. Two compartments were required to fit Mn kinetic data for olfactory epithelium and lung input compartments. Aggregation of several organ dynamic responses was also accomplished, thereby simplifying parts of the model. Inspection of the plots in the Dorman et al.'s (2002a) data indicated that data from pancreas, testes, and kidney (P-T-K) had qualitatively very similar kinetics and thus were combined (summed) and represented as an aggregate P-T-K compartment. Data sets from brain-resto (B-resto) and olfactory tract and tubercle (OTT) also had qualitatively similar kinetics. These two were combined because of their kinetic similarity and because exchange between the compartments were sufficiently faster than the rest of the model, and not observable during the several days experiment. These preliminary computations helped generate the parsimonious dynamic system model structure shown in Figure 1, which includes two compartments for the lung, all to be quantified in two steps, as described below.

Exogenous input

Dorman et al. (2002a) used a 90 min exposure to an aerosol of $^{54}MnHPO_4$. Because the overall data was collected over a 21 day period, this input was modeled as a bolus (impulse function) at time zero. Input in mass was not reported. Our fastest exponential was back extrapolated to time zero from W^{3}DIMSUM fitting results, for both the olfactory epithelium and the lungs, to calculate the mass value for our inputs. This gave bolus inputs of 0.04 and 1.4 μg into olfactory and lung submodels, respectively.

Olfactory submodel

The olfactory transport hypothesis suggests that Mn is transported transneuronally in an activity dependent fashion. Based on brain circuitry in rats, it was assumed that Mn transport from the olfactory bulb to B-Resto/OTT was unidirectional, making the

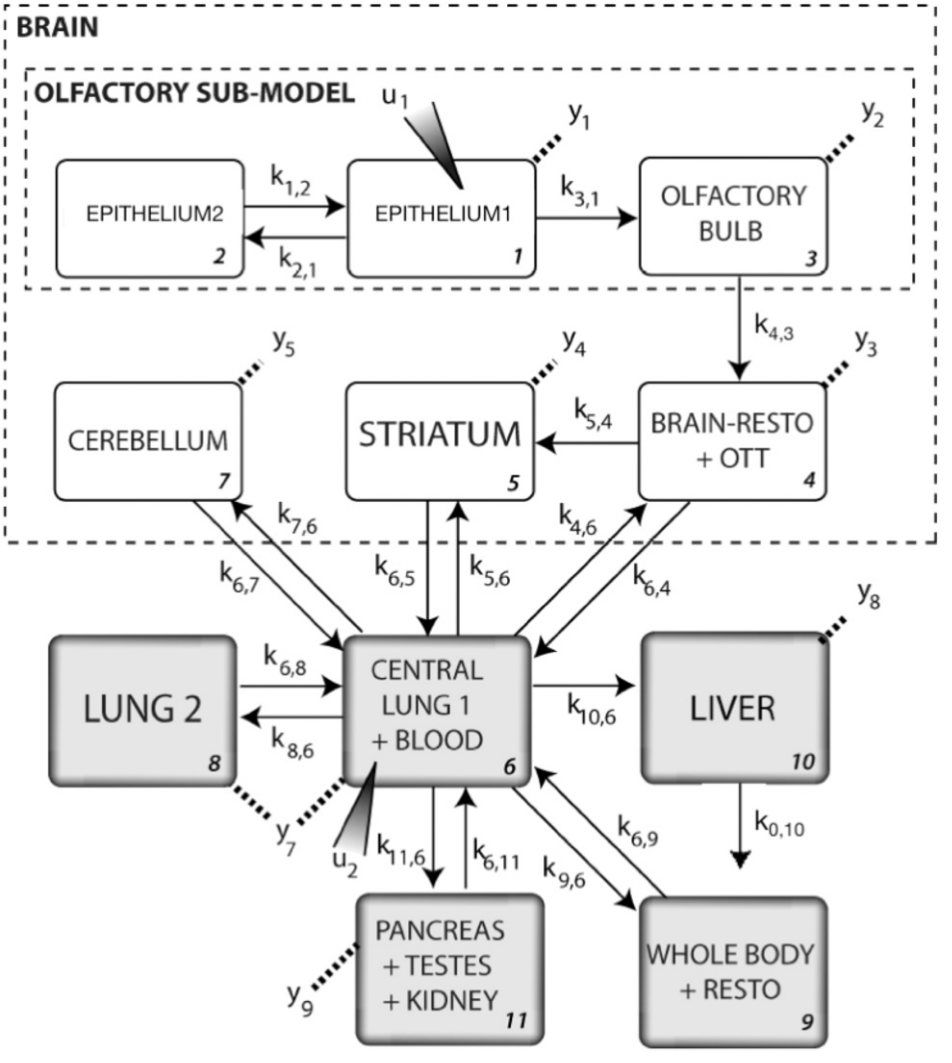

Figure 1. Whole-body pbtk model structure. Shown are the olfactory submodel consisting of olfactory epithelium 1 (EP1), olfactory epithelium 2 (EP2), and olfactory bulb (BULB) (boxed in); brain compartments consisting of olfactory submodel components, as well as Striatum, Cerebellum, and Brain-resto/Olfactory Tract and Tubercle (B-resto/OTT) (boxed in), the whole-body components include Central + Lung 1 + Blood, Lung 2, Rest of body (Resto), and Pancreas/Testes/Kidney (P-T-K), and Liver, (gray). Inputs u_1 into EP1 and u_2 into Central+Lung1+Blood are shown with darkened arrows. Rate constants (k_{ij} day^{-1}) are shown on arrows. EP2 and Lung2 were needed to accommodate best 2-exponential fits to epithelium and lung data in preliminary analyses (see text).

olfactory submodel separable (Zeman 1963). This submodel consists of two compartments for the olfactory epithelium, and one for the olfactory bulb. The olfactory submodel equations describing masses of Mn in compartments q_1 and q_2, with fractional rate constants, k_{ij}, are:

$$\begin{aligned} &\text{EPITHELIUM1} \quad \tfrac{dq_1}{dt} = k_{12}q_2 - (k_{21} + k_{31})q_1 + u_1; \\ &\text{EPITHELIUM2} \quad \tfrac{dq_2}{dt} = k_{21}q_1 - k_{12}q_2. \end{aligned} \tag{2a, b}$$

This submodel was implemented and optimally fitted to the olfactory data, as shown in Figure 2 (a–b), using SAAMII software (University of Washington, Department of Biomedical Engineering), with a Rosenbrock integrator and relative data weighting.

Whole system model quantification

As noted earlier, data from the testes, kidney, and pancreas displayed similar kinetics, and were combined in a single compartment, P-T-K. Two additional compartments representing the remainder of the body (resto) were added to allow for other tissues that concentrate Mn in small amounts such as bone and muscle. Mn is transported actively into the liver via transferrin (Andersen, Gearhart, and Clewell 1999). Transport into the liver is assumed to saturate at toxic levels (Nong et al. 2008; Teeguarden et al. 2007b; Teeguarden et al. 2007c). Flux into the liver was modeled as a first order Hill function. A tilde was used to indicate that this parameter is nonlinear:

$$\tilde{k}_{10,6} = \frac{v_{\max}}{k_m + q_6}. \tag{3}$$

The whole-body PBTK model equations describing mass of Mn in compartment n, q_n, with linear fractional rate constants k and nonlinear fractional rate constants $\tilde{k}$ are:

$$\begin{aligned}
&\text{OLFACTORY_BULB} && \frac{dq_3}{dt} = k_{31}q_1 - k_{43}q_3;\\
&\text{BRAIN} - \text{RESTO} + \text{OTT} && \frac{dq_4}{dt} = k_{43}q_3 - (k_{54} + k_{64})q_4 + k_{46}q_6;\\
&\text{STRIATUM} && \frac{dq_5}{dt} = k_{54}q_4 + k_{56}q_6 - k_{65}q_5;\\
&\text{CENTRAL_LUNG1} + \text{BLOOD} && \frac{dq_6}{dt} = u_2 + k_{64}q_4 + k_{65}q_5 + k_{67}q_7 + k_{68}q_8 + k_{69}q_9\\
&&& \quad + k_{6,11}q_{11} - (k_{46} + k_{56} + k_{76} + k_{86} + k_{96} + k_{10,6}\\
&&& \quad + k_{11,6})q_6;\\
&\text{CEREBELLUM} && \frac{dq_7}{dt} = k_{76}q_6 - k_{67}q_7;\\
&\text{LUNG2} && \frac{dq_8}{dt} = k_{86}q_6 - k_{68}q_8;\\
&\text{WHOLE_BODY} + \text{RESTO} && \frac{dq_9}{dt} = k_{96}q_6 - k_{69}q_9;\\
&\text{LIVER} && \frac{dq_{10}}{dt} = \tilde{k}_{10,6}q_6 - k_{0,10}q_{10};\\
&\text{PANCREAS} + \text{TESTES} + \text{KIDNEY} && \frac{dq_{11}}{dt} = k_{11,6}q_6 - k_{6,11}q_{11}.
\end{aligned} \tag{4a–i}$$

Optimized parameter values from the olfactory submodel were fixed and the PBTK model (Figure 1) was implemented and quantified using SAAMII. Structural identifiability of the model with our reduced parameter set was established numerically, as part of the numerical optimization procedure, which yielded finite variance estimates for all optimized parameters.

Pool size and mass flux analysis

At approximately 500 days, each compartment had reached a final steady state value, in response to a constant infusion (step) input equal to 0.5% of the experimental value, thus

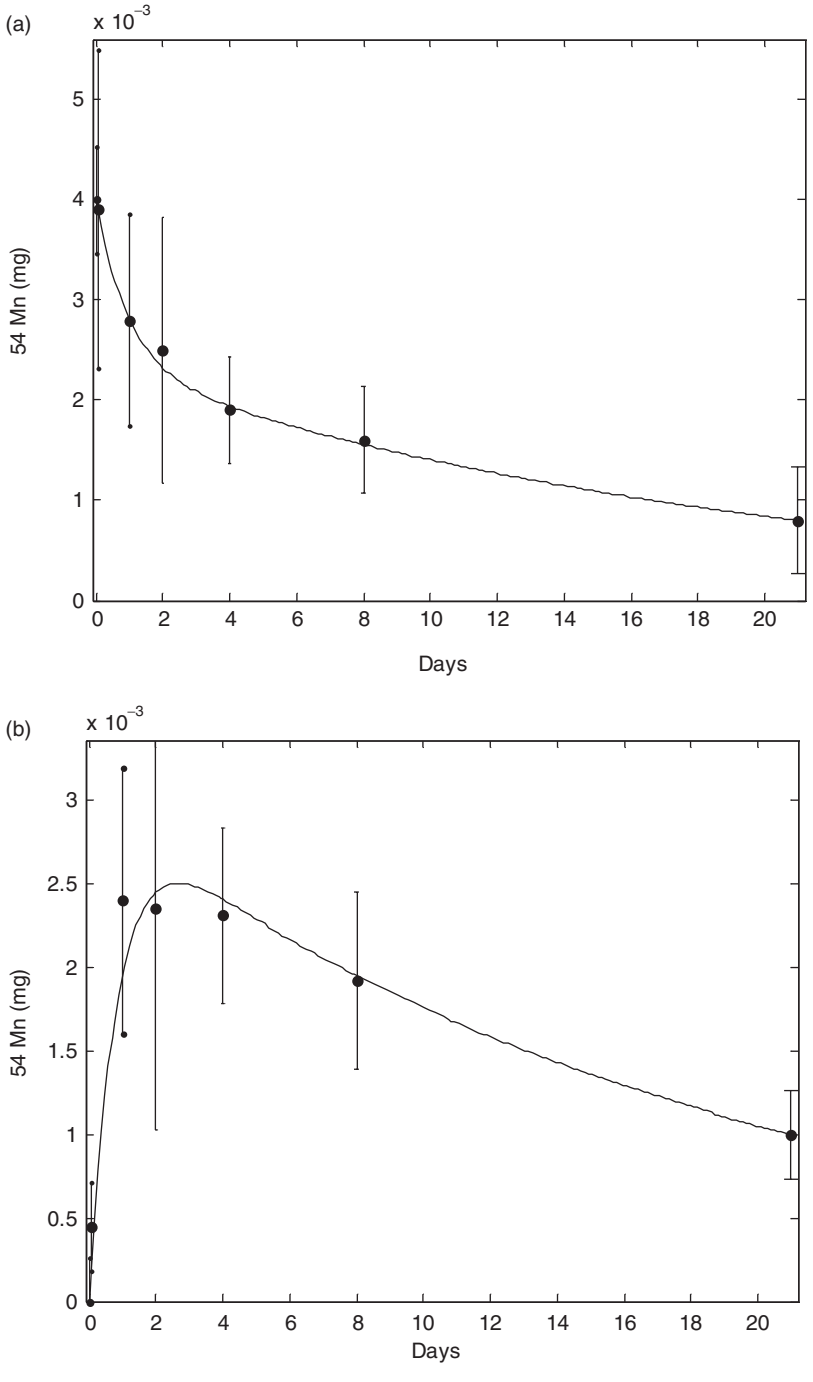

Figure 2. Optimally fitted olfactory submodel data with standard deviations (SD) plotted for: (a) Olfactory Epithelium (EP1) (b) Olfactory bulb (BULB), and optimally fitted whole-body toxicokinetic data for (c) B-resto/OTT, (d) Striatum, (e) Cerebellum, (f) Central + Lung1 + Blood (g) liver, and (h) Pancreas/Testes/Kidney (P-T-K).

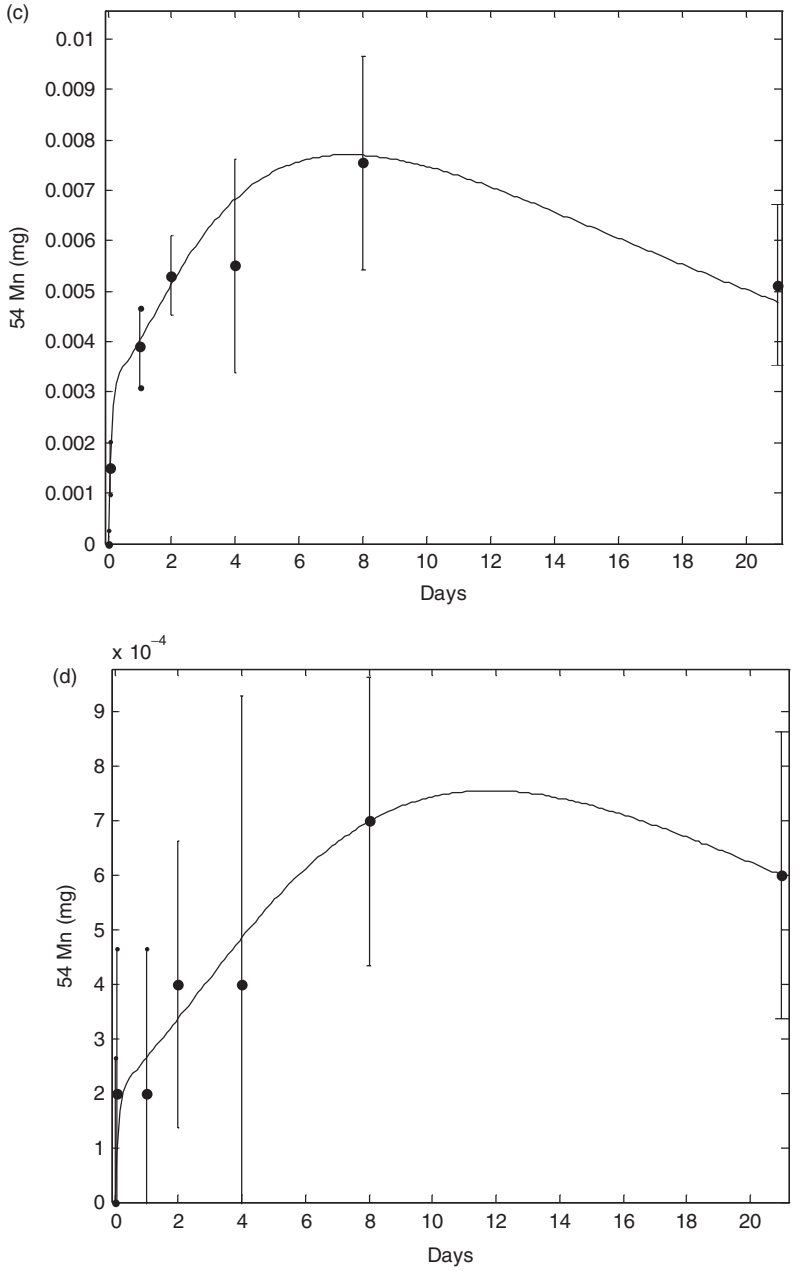

Figure 2. Continued.

keeping the total input amounts (integral) equal to the experimental values. The percent pool size, % $q_{i\mathrm{SS}}$ was calculated at steady state for compartment, i, as:

$$\%\ q_{i\mathrm{SS}} = \left(\frac{q_{i\mathrm{SS}}}{\sum_i^n q_{i\mathrm{SS}}}\right) \times 100, \tag{5}$$

where, $q_{i\mathrm{SS}}$ represents the steady state mass of Mn in compartment.

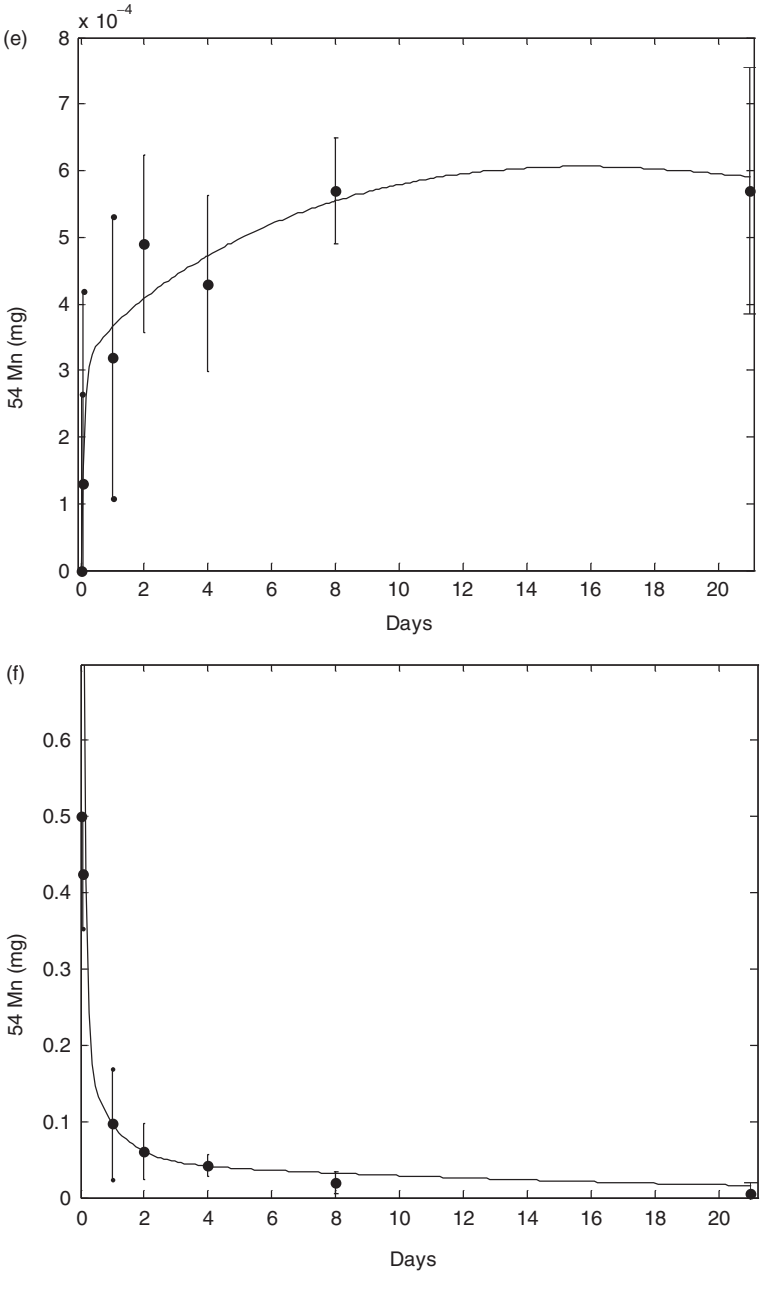

Figure 2. Continued.

Sensitivity analysis

Integrated relative parameter sensitivities in our model were computed to assess how robust model results are to changes in our optimized parameter estimates. The primary goal is to understand Mn accumulation in striatum over time. Thus, the area under the curve (AUC) was selected as the test objective of sensitivity, because it represents

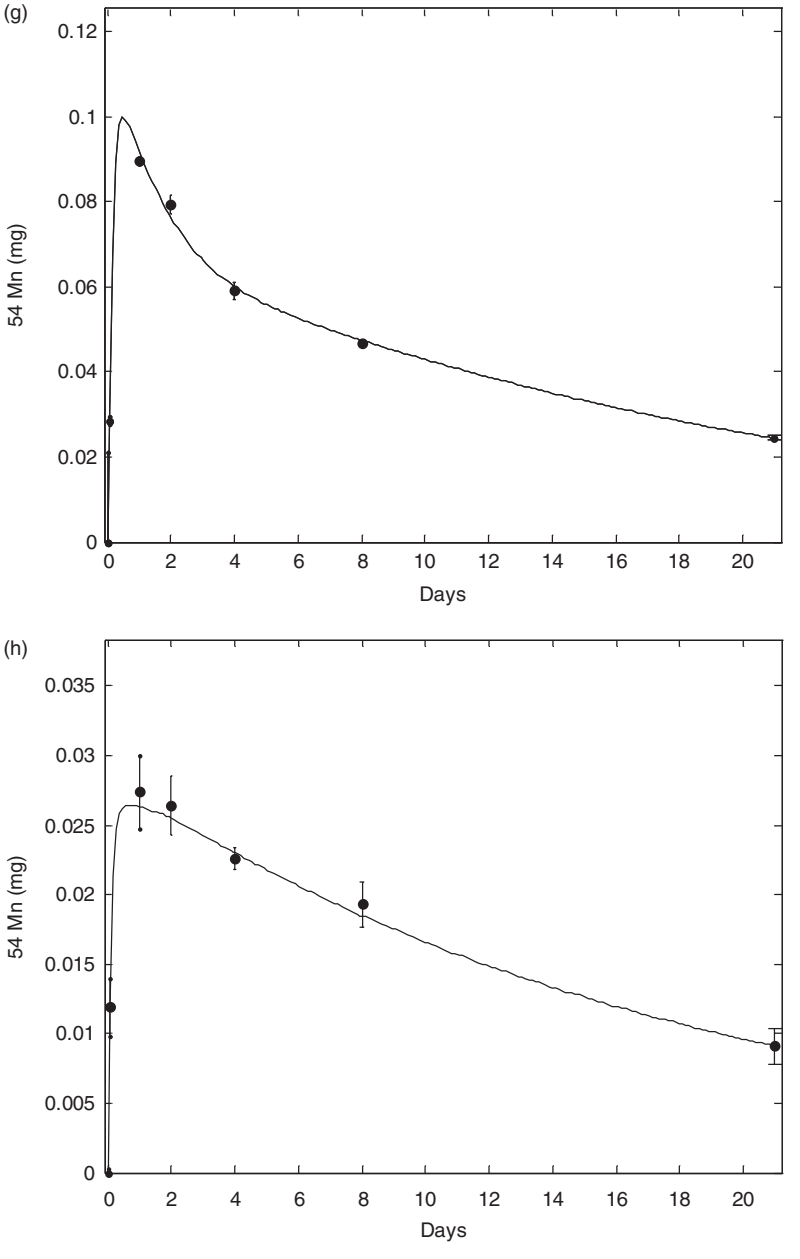

Figure 2. Continued.

accumulated Mn over time. The relative parameter sensitivities, S, of the integral of striatum response, $\mathrm{AUC}_{\mathrm{STRIATUM}}$, were computed, for 10% variations ($\Delta p = 0.1$) in parameters p_j (DiStefano, Stubberud, and Williams 1990) from:

$$S_{p_j}^{\mathrm{AUC}} = \left(\frac{\Delta \mathrm{AUC}_i(t,p^{\mathrm{o}})}{\Delta p_j}\right)\left(\frac{p_j^{\mathrm{o}}}{\mathrm{AUC}_i(t,p^{\mathrm{o}})}\right). \tag{6}$$

Table 1. Parameter estimates for olfactory submodel.

Parameter	Description	MEAN (per day)	SD	% CV
k_{43}	BULB to Brain-Resto/OTT	0.74	0.15	20.4
k_{12}	EP2 to EP1	0.64	0.13	20.2
k_{21}	EP1 to EP2	0.39	0.12	29.4
k_{31}	EP1 to BULB	0.09	0.01	6.6

Results

Olfactory submodel

Optimally fitted output results for the olfactory submodel (Figure 1a) are illustrated in Figure 2(a–c). Each compartment of the olfactory submodel fitted to the data clearly captures the data trends well by both qualitative and quantitative measures. The fits for both olfactory epithelium (EP1) and olfactory bulb (BULB (pass through the data within one standard deviation (SD) (Figures 2a and b)). Parameter coefficients of variation (CVs), given in Table 1, are relatively small, indicating robust estimates for the olfactory submodel parameters.

Whole system model quantification

Graphs of Brain-resto + OTT, striatum, and cerebellum compartments fitted to the data are shown in Figures 2 (c–d), with parameter estimates given in Table 2. All are within a single standard deviation from the mean data point, as above, demonstrating that the brain submodel fits the data well. The model fitted the last two striatum data points very closely, this is important because Mn mass in striatum was predicatively simulated out to longer time points. The remaining body compartments, Central+Lung1+Blood, liver, and P-T-K, fitted to the data are shown in Figures 2(f–h). The CVs average 11%, with a max of 31%.

Sensitivity analysis

Sensitivities of the area under the curve for striatum ($AUC_{STRIATUM}$) to most parameters were quite low (all but one $<11\%$), with the key sensitivity being 31% for a 10% perturbation in k_{46}, the fractional rate of Mn transfer to striatum from the central compartment (see Table 3).

Mn pathways to striatum: direct olfactory versus indirect pulmonary route

The contributions of the olfactory (direct) and pulmonary (indirect) routes for Mn reaching striatum were assessed as follows. $AUC_{STRIATUM}$, i.e., the total accumulated Mn, was computed in striatum 21 days (the duration of the experiment) and also at 50, 100, and 200 days, with both inputs u_1 and u_2 set to the values used in the model quantification studies (0.04 and 1.4 mg Mn, respectively). The indirect (pulmonary) contribution ($\sim$48%) was computed by setting the input to the olfactory epithelium $u_1 = 0$, keeping the input to plasma/lung (u_2) constant at its experimental value (1.4 mg Mn).

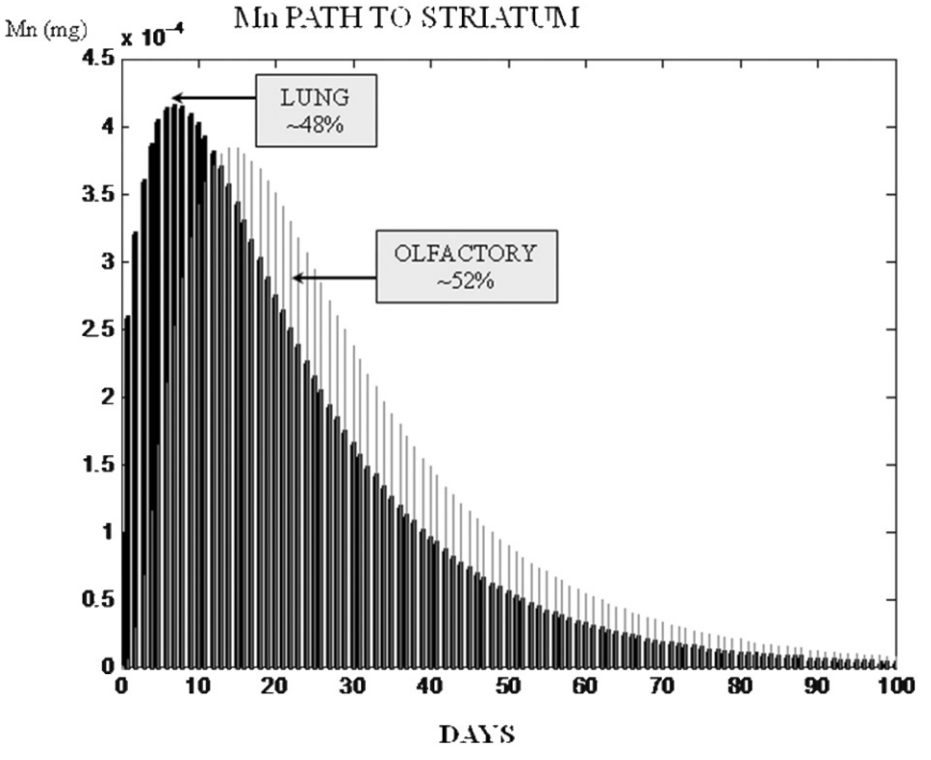

Figure 3. Lung (~48%) in black, and Olfactory in grey (~52%) contributions to the area under the curve (AUC) of Mn in rat striatum at 100 days. Thus, in steady-state, contributions of each pathway to Mn accumulation in rat striatum are about equal.

Similarly, the olfactory contribution (~52%) was determined by setting $u_2 = 0$. Results ranged from ~54–46% at 21 days to 52–48% at 200 days, shown in Figure 3 at 100 days. The separate contributions are also computable by subtraction of either one from the total, given superposition of inputs is valid, which was confirmed.

Clearance from striatum

Additionally, Mn in rat striatum was simulated over 100 days in response to either acute or chronic exposure. In the Dorman et al. (2002a) experiment, rats were exposed to 0.39 mg 5^4 Mn/m^3. The original input was multiplied by 2.6 to reach acute (bolus) exposure levels, or concentrations greater than 1 mg (Mn/m^3) (Dorman et al. 2004). Chronic exposure typically occurs in the occupational setting (e.g. welders, miners, etc.), and may only be present in small amounts. An input of one one-hundredth of the acute value was selected for the chronic case. A constant infusion for 5 days, followed by no infusion for 2 days was used to mimic the work-week. The first infusion pulse began at time zero, and pulses repeated for the 100-day simulation. Results (Figure 4) demonstrate that most Mn in rat striatum appears to clear within 100 days following a single acute (bolus) exposure. For the chronic input, Mn in striatum approaches a constant level.

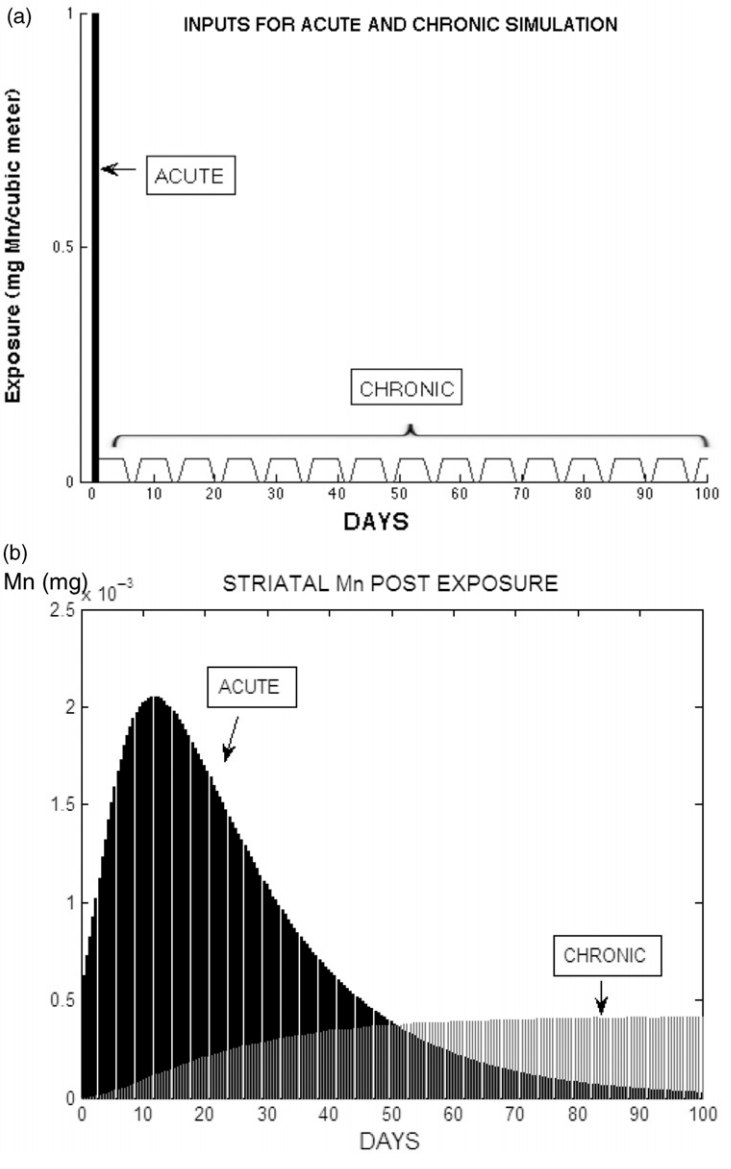

Figure 4. (a) Illustration of the acute bolus input (black) and chronic (pulsed) input simulations. The acute case was modeled as a bolus impulse function occurring at time zero (1 mg Mn/m^3 (Dorman et al. 2002a) experimental values multiplied by 2.6). The chronic case was an extended pulse exposure, (1% of acute values pulsed for 5 days on, 2 days off to mimic the work-week. This 7-day cycle repeated for the 100-day simulation. (b) Simulated dynamics for striatal Mn clearance over 100 days following either an acute (1 mg Mn/m^3) bolus exposure at time zero (Dorman et al. 2002a) experimental values multiplied by 2.6) – in black; or a chronic exposure in gray that might occur in an occupational setting.

Pool size and mass flux analysis

The steady state distribution of Mn in the 11 compartments and the intercompartmental mass fluxes (μg Mn/day) are shown in Figure 5. Notably, the liver is known to actively concentrate Mn and was found to have the largest pool size (~6.7%) of the

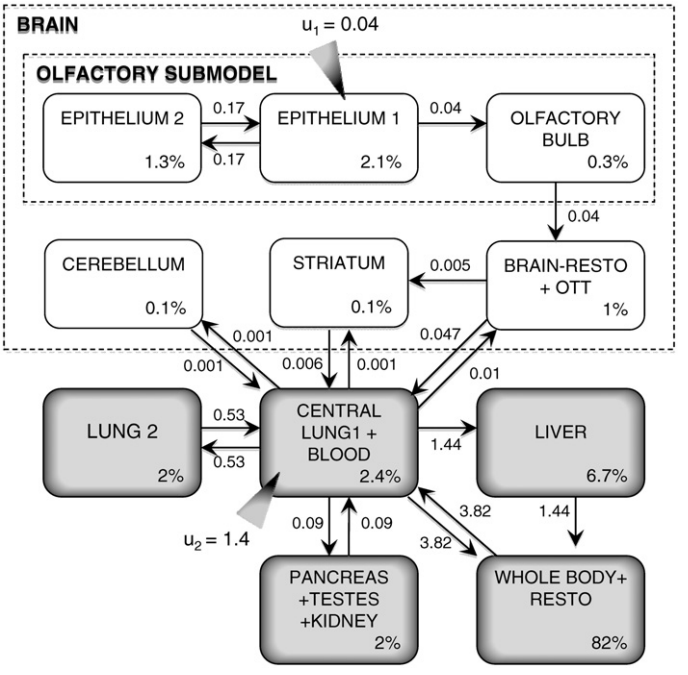

Figure 5. Whole-body Mn distribution (%) and Mn mass flux compartment interchange rates in rats. Pool sizes in% of total body Mn. Mass fluxes per day (μMn/day units) shown on arrows.

measured organs. Unmeasured resto contained (~82%) of the total body pool. Striatum accumulated ~0.1% of total Mn. Cerebellum, with a volume ~100 times that of striatum, (Andersson et al. 2002; Swanson 1995) also accumulated ~0.1% Mn.

Discussion

Dorman et al. (2002a) provided extensive rat organ kinetic data, enough to successfully quantify the 11-compartment whole-body PBTK model of Mn distribution and clearance presented herein. Other published models provide an understanding of various aspects of Mn distribution and clearance in rats (Brenneman et al. 2000; Franzone et al. 1982; House and Wastney 1997; Nathanson et al. 1984; Nong et al. 2008; Teeguarden et al. 2007a; Teeguarden et al. 2007b; Teeguarden et al. 2007c). The model developed here goes further by quantifying Mn distribution more comprehensively and, importantly, also quantifies route of transport to the basal ganglia and predicts Mn levels in rat striatum in response to different simulated inputs. Both modeled olfactory and pulmonary routes were shown to contribute roughly equally, on early and late time scales respectively.

Manganese route to brain: direct (olfactory) or indirect (lung/plasma)

For years, controversy has surrounded the issue of whether Mn enters striatum directly via the olfactory route or indirectly via the lung/plasma and then crosses the blood-CSF or BBB. It is known that metals including copper, iron, mercury, and zinc cross the BBB via

Table 2. Whole-body parameter estimates.

Parameter	Description	MEAN (per day)	SD	% CV
$k_{0,10}$	Liver clearance	1.02	0.020	2.0
k_{43}	Olfactory Bulb to Brain-Resto + OTT	0.699	0.110	15.7
k_{46}	Central to Brain-Resto + OTT	0.023	0.001	3.9
k_{54}	Brain-Resto + OTT to Striatum	0.024	0.005	20.8
k_{56}	Central Lung 1 + Blood to Striatum	0.0014	0.0004	29.0
k_{64}	Brain-Resto/OTT to Central Lung1 + Blood	0.217	0.020	9.2
k_{65}	Striatum to Central Lung1 + Blood	0.251	0.049	19.6
k_{67}	Cerebellum to Central Lung1 + Blood	0.040	0.012	30.9
k_{68}	Lung2 to Central Lung1 + Blood	1.23	0.017	1.4
k_{69}	Resto to Central Lung 1 + Blood	0.218	0.006	2.9
$k_{6,11}$	P-T-K to Central Lung 1 + Blood	0.223	0.010	4.4
k_{76}	Central Lung 1 + Blood to Cerebellum	0.0022	0.0002	8.7
k_{86}	Central Lung 1 + Blood to Lung2	1.06	0.084	7.9
k_{96}	Central Lung1 + Blood to Resto	7.67	0.488	6.4
$k_{11,6}$	Central Lung1 + Blood to P-T-K	0.185	0.010	5.3
K	Hill parameter for efflux to Liver (mg Mn)	0.198	0.015	7.6
V	Hill max velocity parameter for efflux to Liver (mg/day)	0.588	0.024	4.1

Table 3. Percent relative sensitivities (% S_{pj}^{AUC}) for striatum area under the curve ($\mathrm{AUC}_{\mathrm{STRIATUM}}$) in response to a 10% perturbation of all model parameters ($\Delta p_j = 0.1$).

Parameter	Description	% Sensitivity
k_{31}	EP1 to BULB	1
k_{12}	EP2 to EP1	12
k_{21}	EP1 to EP2	12
k_{43}	BULB to Brain-Resto + OTT	31
k_{46}	Central Lung1 + Blood to Brain-Resto + OTT	<1
k_{64}	Brain-Resto + OTT to Central Lung 1 + Blood	<1
k_{54}	Brain-Resto + OTT to Striatum	17
k_{65}	Striatum to Central Lung1 + Blood	27
k_{56}	Central Lung1 + Blood to Striatum	17
k_{67}	Cerebellum to Central Lung1 + Blood	1
k_{76}	Central Lung 1 + Blood to Cerebellum	3
k_{68}	Lung2 to Central Lung1 + Blood	<1
k_{86}	Central Lung1 + Blood to Lung2	1
k_{69}	Whole Body Resto to Central Lung 1 + Blood	1
k_{96}	Central Lung1 + Blood to Whole Body Resto	1
$k_{6,11}$	P-T-K to Central Lung1 + Blood	<1
$k_{11,6}$	Central Lung 1 + Blood to P-T-K	<1
$k_{0,10}$	Leak from Liver	<1
K	Hill parameter for Influx to Liver	4
V	Hill max velocity for influx to Liver	4

carrier mediated transport. Yokel (2002) proposed that Mn enters the brain in a similar fashion. However, others suggested that Mn enters the brain primarily from the nasal cavity followed by activity dependent transneuronal transport in a manner similar to calcium, another divalent cation (Dorman et al. 2002a; Dorman et al. 2006; Leavens et al. 2007). Dendrites of primary olfactory neurons are in contact with the olfactory lumen at

the site of the olfactory epithelium. Mn can be taken up by these dendrites and be transneuronally carried from the lumen to the olfactory bulb and further areas of the brain (Tjalve and Henriksson 1999).

Understanding this issue is paramount for the design of treatments such as chelating therapy and interventions (Gaeta and Hider 2005). Although Dorman et al. (2006) noted a rostro-caudal concentration gradient along the olfactory pathway in rhesus monkeys following airborne exposure to Mn, they were unable to observe higher Mn concentrations in the intervening tissue. Activity mapping and track tracing studies with MEMRI in rats (Koretsky and Silva 2004; Lu et al. 2007; Paulter et al. 2004; Silva et al. 2004) may likely elucidate Mn pathways taken in the olfactory route to reach these deep brain structures.

Mn may cross the blood brain barrier (BBB), blood cerebrospinal fluid barrier (BCSFB), or cross unguarded areas of the brain such as the area postrema when using the indirect lung to blood to brain pathway. At physiologic concentrations, Mn influx into the brain is passive, nonsaturable, and thought to occur primarily through the capillary bed of the BBB (Rabin et al. 1993). In contrast, at higher potentially toxic concentrations, passive influx through the BCSFB is thought to dominate (Murphy et al. 1991; Rabin et al. 1993). The neuroanatomical proximity of the third ventricle to striatum might explain how transport across the BCSFB may provide a means for Mn to reach striatum without accumulating in other brain structures. Small ions and other chemicals like the HIV drug, AZT, are known to cross the blood-CSF barrier (Wu et al. 1992). Further investigations may focus on how Mn enters brain when using the pulmonary route (BBB or BCSFB), and why this ion selectively accumulates in striatum.

Mn in striatum

The half-life of Mn in the rat brain was reported to be 51–74 days (Takeda, Sawashita, and Okada 1995). A shorter half-life in soft tissue and a longer half-life in the skeletal system have been reported (Furchner, Richmond, and Drake 1966). A terminal half-life of ~30 days (Dorman et al. 2001b) and 7 to 30 days in rat whole-body (Lee and Johnson 1988, 1989) and not much longer in humans (Johnson, Lykken, and Korynta 1991; Mahoney and Small 1968) has also been reported. Dorman and others 2001a, 2002a suggest that Mn is primarily concentrated in rat striatum following exposure. However, other work by this same group suggests otherwise (Dorman et al. 2002b). Clearly, age, gender and liver function (Erikson et al. 2004; Hauser et al. 1994) effect clearance rates following either exposure variant.

Recently, Mn has been used in rats as a contrast agent in Mn enhanced MRI (MEMRI) track tracer studies (Lu et al. 2007; Pautler 2004; Silva et al. 2004; Pautler, Mongeau, and Jacobs 2003). MEMRI will likely yield useful experimental data about Mn transport to rat striatum for testing our predictions. Further, extrapolating these imaging studies to humans may indicate how useful MRI scans are at detection of striatal Mn following exposure.

Study limitations

Rats differ from humans in that they are obligatory nose breathers (Dorman et al. 2002a). Thus the olfactory versus pulmonary contributions may be different in humans. Rats also do not develop symptoms of manganism and thus the rat may not be the best experimental model for Mn studies. The PBTK model developed here was based on radioactive Mn

used in the Dorman and others (2002a) study. Nonradioactive Mn may behave differently in tissue, representing another potential limitation in this study.

Model parameters were calculated based on acute input exposure data. Nong and others (2008) noted that Mn models of accumulation should take into account different behaviors for normal (low) intake versus high (toxic) amounts. It is possible that parameter values would differ under chronic exposure conditions. However, both acute and chronic simulated inputs were well above toxic tissue levels, and therefore parameter estimates should be consistent in both acute and chronic toxic conditions.

Conclusions

The goal of this investigation was to quantitatively explore whole-body Mn distribution and – in particular – its accumulation in striatum – in the rat. We accomplished this by developing an 11-compartment whole-body PBTK model of Mn distribution in rats, based on multiorgan rat data. The fully quantified model provided numerous kinetic parameters, including the relative distribution of whole-body Mn for each compartment in response to a constant simulated input of inhaled Mn, and the relative contributions of olfactory and pulmonary pathways. The liver contained the greatest percentage of measured organs (~6.7%), and (~82%) estimated inside unmeasured organs. Both striatum and cerebellum contained (~0.1%) of total Mn, which is notable given that striatum volume is approximately 100 fold less than cerebellum. The percent of olfactory (~52%) and pulmonary (~48%) contribution to Mn in striatum were computed after acute aerosolized exposure. Our simulations predict that clearance from striatum over time was nearly complete after ~100 days following acute exposure ($>1\,\mathrm{mg\,Mn/m^3}$). In a separate simulation of low-level chronic exposure ($\sim 0.01\,\mathrm{mg\,Mn/m^3}$), striatal Mn was saturated and reached an approximately steady value at 100 days. Sensitivities of $\mathrm{AUC_{STRIATUM}}$ to most parameters were quite low (all but one $<11\%$), with the key sensitivity being 31% for a 10% perturbation in k_{46}, the fractional rate of Mn transfer to striatum from the central compartment.

The rat striatum does not accumulate Mn, so the rat is not the best animal model for studying manganism in humans. Nevertheless, the methodology developed in this work should be directly applicable to animal data that does better reflect the human condition and, ultimately, should be helpful in extrapolation to the human.

Acknowledgments

This study was supported in part by the National Science Foundation (NSF) Integrative Graduate Education and Research Traineeship (IGERT) program, and the UCLA NIH Neuroimaging Training Program (NITP), and the University of California, Los Angeles Graduate Research Mentorship Program.

References

Andersen, M.E., J.M. Gearhart, and H.J. Clewell 3rd. 1999. Pharmacokinetic data needs to support risk assessments for inhaled and ingested manganese. *Neurotoxicology* 20: 161–71.

Andersson, C., R.M. Hamer, C.P. Lawler, R.B. Mailman, and J.A. Lieberman. 2002. Striatal volume changes in the rat following long-term administration of typical and atypical antipsychotic drugs. *Neuropsychopharmacology* 27: 143–51.

Ascherio, A., H. Chen, M.G. Weisskopf, E. O'Reilly, M.L. McCullough, E.E. Calle, M.A. Schwarzschild, and M.J. Thun. 2006. Pesticide exposure and risk for Parkinson's disease. *Annals of Neurology* 60: 197–203.

Aschner, J.L., and M. Aschner. 2005. Nutritional aspects of manganese homeostasis. *Molecular Aspects of Medicine* 26: 353–62.

Baldereschi, M., M. Inzitari, P. Vanni, A. Di Carlo, and D. Inzitari. 2007. Pesticide exposure might be a strong risk factor for Parkinson's disease. *Annals of Neurology* 63: 128.

Bock, N.A., F.F. Paiva, G.C. Nascimento, J.D. Newman, and A.C. Silva. 2008. Cerebrospinal fluid to brain transport of manganese in a non-human primate revealed by MRI. *Brain Research* 1198: 160–70.

Bowler, R.M., S. Gysens, E. Diamond, S. Nakagawa, M. Drezgic, and H.A. Roels. 2006. Manganese exposure: Neuropsychological and neurological symptoms and effects in welders. *Neurotoxicology* 27: 315–26.

Brenneman, K.A., B.A. Wong, M.A. Buccellato, E.R. Costa, E.A. Gross, and D.C. Dorman. 2000. Direct olfactory transport of inhaled manganese ((54)MnCl(2)) to the rat brain: Toxicokinetic investigations in a unilateral nasal occlusion model. *Toxicology and Applied Pharmacology* 169: 238–48.

Calonder, C., P.I. Wurtenberger, R.P. Maguire, R. Pellikka, and K.L. Leenders. 1999. Kinetic modeling of 52Fe/52mMn-citrate at the blood-brain barrier by positron emission tomography. *Journal of Neurochemistry* 73: 2047–55.

Clodfelder, B.J., C. Chang, and J.B. Vincent. 2004. Absorption of the biomimetic chromium cation triaqua-mu3-oxo-mu-hexapropionatotrichromium(III) in rats. *Biological Trace Element Research* 98: 159–69.

Couper, J. 1837. On the effects of black oxide of manganese when inhaled into the lungs. *British Annals of Medical Pharmacology* 1: 41–32.

Crossgrove, J.S., D.D. Allen, B.L. Bukaveckas, S.S. Rhineheimer, and R.A. Yokel. 2003. Manganese distribution across the blood-brain barrier I. Evidence for carrier-mediated influx of managanese citrate as well as manganese and manganese transferrin. *Neurotoxicology* 24: 3–13.

Crossgrove, J.S., and R.A. Yokel. 2004. Manganese distribution across the blood-brain barrier III. The divalent metal transporter-1 is not the major mechanism mediating brain manganese uptake. *Neurotoxicology* 25: 451–60.

Crossgrove, J.S., and R.A. Yokel. 2005. Manganese distribution across the blood-brain barrier IV. Evidence for brain influx through store-operated calcium channels. *Neurotoxicology* 26: 297–307.

Crossgrove, J., and W. Zheng. 2004. Manganese toxicity upon overexposure. *NMR in Biomedicine* 17: 544–53.

DiStefano III, J.J., A.R. Stubberud, and I.J. Williams. 1990. *Schaum's outline series theory and problems of feedback and control systems*. 2nd ed. New York: McGraw-Hill, Inc.

Dobson, A.W., K.M. Erikson, and M. Aschner. 2004. Manganese neurotoxicity. *Annals of the New York Academy of Sciences* 1012: 115–28.

Dorman, D.C., K.A. Brenneman, A.M. McElveen, S.E. Lynch, K.C. Roberts, and B.A. Wong. 2002a. Olfactory transport: A direct route of delivery of inhaled manganese phosphate to the rat brain. *Journal of Toxicology and Environmental Health. Part A* 65: 1493–511.

Dorman, D.C., M.F. Struve, H.J. Clewell III, and M.E. Andersen. 2006. Application of pharmacokinetic data to the risk assessment of inhaled manganese. *Neurotoxicology* 27: 752–64.

Dorman, D.C., M.F. Struve, R.A. James, M.W. Marshall, C.U. Parkinson, and B.A. Wong. 2001a. Influence of particle solubility on the delivery of inhaled manganese to the rat brain: Manganese sulfate and manganese tetroxide pharmacokinetics following repeated (14-day) exposure. *Toxicology and Applied Pharmacology* 170: 79–87.

Dorman, D.C., M.F. Struve, R.A. James, B.E. McManus, M.W. Marshall, and B.A. Wong. 2001b. Influence of dietary manganese on the pharmacokinetics of inhaled manganese sulfate in male CD rates. *Toxicological Sciences* 60: 242–51.

Dorman, D.C., M.F. Struve, E.A. Gross, B.A. Wong, and P.C. Howroyd. 2004. Sub-chronic inhalation of high concentrations of manganese sulfate induces lower airway pathology in rhesus monkeys. *Respiratory Research* 6: 121.

Dorman, D.C., M.F. Struve, and B.A. Wong. 2002b. Brain manganese concentrations in rats following manganese tetroxide inhalation are unaffected by dietary manganese intake. *Neurotoxicology* 23: 185–95.

Dote, T., K. Adachi, E. Yamadori, M. Imanishi, H. Tsuji, E. Tanida, and K. Kono. 2008. Abnormalities in cadmium fluoride kinetics in serum, bile, and urine after single intravenous administration of toxic doses to rats. *Journal of Occupational Health* 50: 339–47.

Erikson, K.M., A.W. Dobson, D.C. Dorman, and M. Aschner. 2004. Manganese exposure and induced oxidative stress in the rat brain. *The Science of the Total Environment* 334–335: 409–416.

Farris, E.J., and J.H. Griffith. 1949. *The rat in laboratory investigation*. 2nd ed. Philadelphia: JB Lippincott Co.

Furchner, J.E., C.R. Richmond, and G.A. Drake. 1966. Comparative metabolism of radionuclides in mammals. Three retention of manganese-54 in the mouse, rat, monkey, and dog. *Health Physics* 12: 1415–23.

Gaeta, A., and R.C. Hider. 2005. The crucial role of metal ions in neurodegeneration: The basis for a promising therapeutic strategy. *British Journal of Pharmacology* 146: 1041–59.

Gentry, P.R., T.R. Covington, S. Mann, A.M. Shipp, J.W. Yager, and H.J. Clewell III. 2004. Physiologically based pharmacokinetic modeling of arsenic in the mouse. *Journal of Toxicology and Environmental Health. Part A* 67: 43–71.

Gianutsos, G., G.R. Morrow, and J.B. Morris. 1997. Accumulation of manganese in rat brain following intranasal administration. *Fundamental and Applied Toxicology* 37: 102–5.

Hack, C.E., T.R. Covington, G. Lawrence, A.M. Shipp, R. Gentry, J. Yager, and H.J. Clewell III. 2007. A pharmacokinetic model of the intracellular dosimetry of inhaled nickel. *Journal of Toxicology and Environmental Health. Part A* 70: 445–64.

Harless, C., and J.J. Distefano III. 2005. Automated expert multiexponential biomodeling interactively over the internet. *Computer Methods and Programs in Biomedicine* 79: 169–78.

Hauser, R.A., T.A. Zesiewicz, A.S. Rosemurgy, C. Martinez, and C.W. Olanow. 1994. Manganese intoxication and chronic liver failure. *Annals of Neurology* 36: 871–5.

House, W.A., and M.E. Wastney. 1997. Compartmental analysis of zinc kinetics in mature male rats. *The American Journal of Physiology* 273: R1117–R1125.

Johnson, P.E., G.I. Lykken, and E.D. Korynta. 1991. Absorption and biological half-life of intrinsic and extrinsic 54 Mn tracers from foods of plant origin. *The Journal of Nutrition* 121: 711–7.

Kaiser, J. 2003. Manganese: A high-octane dispute. *Science* 300: 926–8.

Kim, Y. 2006. Neuroimaging in manganism. *Neurotoxicology* 27: 369–72.

Koretsky, A.P., and A.C. Silva. 2004. Manganese-enhanced magnetic resonance imaging (MEMRI). *NMR in Biomedicine* 17: 527–31.

Kuhn, W., R. Winkel, D. Woitalla, S. Meves, H. Przuntek, and T. Müller. 1998. High prevalence of parkinsonism after occupational exposure to lead-sulfate batteries. *Neurology* 50: 1885–6.

Leavens, T.L., D. Rao, M.E. Andersen, and D.C. Dorman. 2007. Evaluating transport of manganese from olfactory mucosa to striatum by pharmacokinetic modeling. *Toxicological Sciences* 97: 265–78.

Lee, D.Y., and P.E. Johnson. 1988. Factors affecting absorption and excretion of 54Mn in rats. *The Journal of Nutrition* 118: 1509–16.

Lee, D.Y., and P.E. Johnson. 1989. 54Mn absorption and excretion in rats fed soy protein and casein diets. *Proceedings of the Society for Experimental Biology and Medicine* 190: 211–6.

Lu, H., Z.X. Xi, L. Gitajn, W. Rea, Y. Yang, and E.A. Stein. 2007. Cocaine-induced brain activation detected by dynamic manganese-enhanced magnetic resonance imaging (MEMRI). *Proceedings of the National Academy of Sciences of the USA* 104: 2489–94.

Mahoney, J.P., and W.J. Small. 1968. Studies on manganese 3. The biological half-life of radiomanganese in man and factors which affect this half-life. *The Journal of Clinical Investigation* 47: 643–53.

Murphy, V.A., K.C. Wadhwani, Q.R. Smith, and S.I. Rapoport. 1991. Saturable transport of manganese(II) across the rat blood-brain barrier. *Journal of Neurochemistry* 57: 948–54.

Nong, A., J.G. Teeguarden, H.J. Clewell III, D.C. Dorman, and M.E. Andersen. 2008. Pharmacokinetic modeling of manganese in the rat IV: Assessing factors that contribute to brain accumulation during inhalation exposure. *Journal of Toxicology and Environmental Health. Part A* 71: 413–26.

O'Flaherty, E.J. 1998. Physiologically based models of metal kinetics. *Critical Reviews in Toxicology* 28: 271–317.

Pautler, R.G. 2004. In vivo, trans-synaptic tract-tracing utilizing manganese-enhanced magnetic resonance imaging (MEMRI). *NMR in Biomedicine* 17: 595–601.

Pautler, R.G., R. Mongeau, and R.E. Jacobs. 2003. In vivo trans-synaptic tract tracing from the murine striatum and amygdala utilizing manganese enhanced MRI (MEMRI). *Magnetic Resonance in Medicine* 50: 33–9.

Rabin, O., L. Hegedus, J.M. Bourre, and Q.R. Smith. 1993. Rapid brain uptake of manganese(II) across the blood-brain barrier. *Journal of Neurochemistry* 61: 509–17.

Rabinowitz, M. 1998. Historical perspective on lead biokinetic models. *Environmental Health Perspectives* 106 (Suppl 6): 1461–5.

Shinotoh, H., B.J. Snow, N.S. Chu, C.C. Huang, C.S. Lu, C. Lee, H. Takahashi, and D.B. Calne. 1997. Presynaptic and postsynaptic striatal dopaminergic function in patients with manganese intoxication: A positron emission tomography study. *Neurology* 48: 1053–6.

Silva, A.C., J.H. Lee, I. Aoki, and A.P. Koretsky. 2004. Manganese-enhanced magnetic resonance imaging (MEMRI): Methodological and practical considerations. *NMR in Biomedicine* 17: 532–43.

Swanson, L.W. 1995. Mapping the human brain: Past, present, and future. *Trends in Neurosciences* 18: 471–4.

Takeda, A., J. Sawashita, and S. Okada. 1995. Biological half-lives of zinc and manganese in rat brain. *Brain Research* 695: 53–8.

Teeguarden, J.G., D.C. Dorman, T.R. Covington, H.J. Clewell III, and M.E. Andersen. 2007a. Pharmacokinetic modeling of manganese. I. Dose dependencies of uptake and elimination. *Journal of Toxicology and Environmental Health. Part A* 70: 1493–504.

Teeguarden, J.G., D.C. Dorman, A. Nong, T.R. Covington, H.J. Clewell III, and M.E. Andersen. 2007b. Pharmacokinetic modeling of manganese. II. Hepatic processing after ingestion and inhalation. *Journal of Toxicology and Environmental Health. Part A* 70: 1505–14.

Teeguarden, J.G., J. Gearhart, H.J. Clewell III, T.R. Covington, A. Nong, and M.E. Andersen. 2007c. Pharmacokinetic modeling of manganese. III. Physiological approaches accounting for background and tracer kinetics. *Journal of Toxicology and Environmental Health. Part A* 70: 1515–26.

Thompson, K., R. Molina, T. Donaghey, J.D. Brain, and M. Wessling-Resnick. 2006. The influence of high iron diet on rat lung manganese absorption. *Toxicology and Applied Pharmacology* 210: 17–23.

Tjalve, H., and J. Henriksson. 1999. Uptake of metals in the brain via olfactory pathways. *Neurotoxicity* 20: 181–95.

Wang, J.D., C.C. Huang, Y.H. Hwang, J.R. Chiang, J.M. Lin, and J.S. Chen. 1989. Manganese induced parkinsonism: An outbreak due to an unrepaired ventilation control system in a ferromanganese smelter. *British Journal of Industrial Medicine* 46: 856–9.

Wu, X., G. Yuan, C.M. Brett, A.C. Hui, and K.M. Giacomini. 1992. Sodium-dependent nucleoside transport in choroid plexus from rabbit. Evidence for a single transporter for purine and pyrimidine nucleosides. *The Journal of Biological Chemistry* 267: 8813–8.

Yokel, R.A. 2002. Brain uptake, retention, and efflux of aluminum and manganese. *Environmental Health Perspectives* 110 (Suppl 5): 699–704.

Yokel, R.A., and J.S. Crossgrove. 2004. Manganese toxicokinetics at the blood-brain barrier. *Research Report (Health Effects Institute)* 7–58; discussion 59–73.

Yokel, R.A., J.S. Crossgrove, and B.L. Bukaveckas. 2003. Manganese distribution across the blood-brain barrier. II. Manganese efflux from the brain does not appear to be carrier mediated. *Neurotoxicology* 24: 15–22.

Zatta, P., R. Lucchini, S.J. van Rensburg, and A. Taylor. 2003. The role of metals in neurodegenerative processes: Aluminum, manganese, and zinc. *Brain Research Bulletin* 62: 15–28.

Zeman, W.J. 1963. *Craigie's neuroanatomy of the rat*. New York: Academic Press, Revised and expanded by Wolfgang Zeman [and] James Robert Maitland Innes.